PROCEEDINGS OF SPIE

Fabrication of waveguide spatial light modulators via femtosecond laser micromachining

Nickolaos Savidis, Sundeep Jolly, Bianca Datta, Thrasyvoulos Karydis, V. Michael Bove

Fabrication of waveguide spatial light modulators via femtosecond laser micromachining

Nickolaos Savidis, Sundeep Jolly, Bianca Datta, Thrasyvoulos Karydis, and V. Michael Bove, Jr.

MIT Media Lab, 77 Massachusetts Ave., Rm. E15-444, Cambridge, MA, United States

ABSTRACT

We have previously introduced an anisotropic leaky-mode modulator as a waveguide-based, acousto-optic solution for spatial light modulation in holographic video display systems. Waveguide fabrication for these and similar surface acoustic wave devices relies on proton exchange of a lithium niobate substrate, which involves the immersion of the substrate in an acid melt. While simple and effective, waveguide depth and index profiles resulting from proton exchange are often non-uniform over the device length or inconsistent between waveguides fabricated at different times using the same melt and annealing parameters. In contrast to proton exchange, direct writing of waveguides has the appeal of simplifying fabrication (as these methods are inherently maskless) and the potential of fine and consistent control over waveguide depth and index profiles. In this paper, we explore femtosecond laser micromachining as an alternative to proton exchange in the fabrication of waveguides for anisotropic leaky-mode modulators.

Keywords: holography, femtosecond laser micromachining, waveguide optics

1. INTRODUCTION

Our group has previously developed a holographic video display based on space-multiplexed, guided-wave acousto-optic spatial light modulation capable of transparent or opaque viewing operation.[1,2] This previous work demonstrated that guided-wave devices based on proton-exchanged lithium niobate can not only be used for inexpensive holographic displays, but also exhibit polarization rotation, allowing noise and undiffracted light to be eliminated with a polarizer, and wavelength division multiplexing, allowing simultaneous red, green, and blue illumination without color filters or spatial/temporal multiplexing.

There are three base elements that comprise the piezoelectric lithium niobate acousto-optic modulator: 1) the anisotropic waveguide, 2) the surface acoustic wave (SAW) transducer, and 3) the prism coupler. Proton exchange has proven to be an affordable method to take advantage of when fabricating the acousto-optic modulator. Waveguide fabrication for these and similar SAW devices relies on proton exchange of a lithium niobate substrate, which involves the immersion of the substrate in an acid melt. While simple and effective, waveguide depth and index profiles resulting from proton exchange are often non-uniform over the device length or inconsistent between waveguides fabricated at different times using the same melt and annealing parameters. In contrast to proton exchange, direct writing of waveguides has the appeal of simplifying fabrication (as these methods are inherently maskless) and the potential of fine and consistent control over waveguide depth and index profiles. We explore femtosecond laser micromachining as an alternative to proton exchange in the fabrication of waveguides for anisotropic leaky-mode modulators. Femtosecond laser micromachining offers a platform where all three base elements of the acousto-optic modulator can be embedded into the lithium niobate. The prism coupler can be replaced with an in-coupling grating that can be added to the surface of the lithium niobate through either an ablation / vaporization approach or through a two-photon additive polymerization process. The SAW transducer can be fabricated with the femtosecond laser again through an ablation and print process. Finally the anisotropic waveguide can be achieved by altering the refractive index within the lithium niobate to create a core / cladding structure that is traditionally observed in optical waveguides. In this paper we address the current femtosecond laser system being developed to address the creation of anisotropic waveguides in lithium niobate wafers.

Corresponding author: nsavidis@media.mit.edu

2. WRITING WITH FEMTOSECOND LASER

Ultrashort pulse widths and extremely high peak intensities of the femtosecond laser can induce strong absorption in transparent materials due to nonlinear multi-photon absorption. Multi-photon absorption enables both surface and internal three dimensional modification and microfabrication of transparent materials. Femtosecond laser processing is a promising technique for fabricating waveguides within a glass substrate as it can directly form 3-D micro structures in the substrate,[3–7] and in particular writing within lithium niobate with femtosecond laser pulses.[8–15] There are, however, upper limits where ablation or vaporization occurs within a material. The process of optically induced damage, ablation, or vaporization of the material is produced by avalanche breakdown, which is the primary mechanism for material degradation with pulsed lasers operating at pulses shorter than 1 μs with intensities in the range of 10^9 W/cm^2 to 10^{12} W/cm^2.[16]
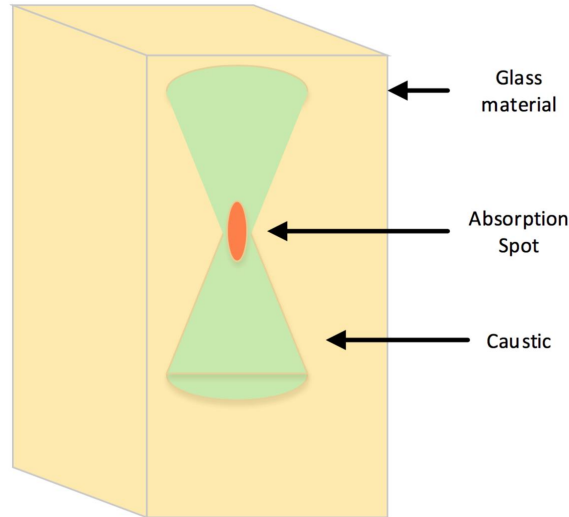

Figure 1. Schematic diagram depicting internal modification of a transparent material by multi-photon absorption or tunneling ionization induced by femtosecond laser irradiation. When a femtosecond laser beam is focused inside a transparent material, absorption is confined to a region near the focal point inside the material, allowing for localized structural fabrication within a transparent medium.

There are two classes of femtosecond micromachining techniques known as parallel processing and serial processing.[17] Parallel processing techniques are femtosecond machining techniques that also require an additional process in parallel to achieve the micromachining technique. This additional processing can include photolithography, soft lithography, UV laser mask patterning, embossing, and micro-injection molding. Serial processing applies micromachining as a direct write process that includes the use of proton and electron beam writing, laser direct writing and xurography. Among the femtosecond micromachining approaches, there are two serial processes that offer direct writing inside a glass material rather than just in the surface. These two approaches are two-photon polymerization (2PP)[18,19] and femtosecond direct writing in glass.[3]

Femtosecond laser machining has been used effectively to induce polymerization reactions through two-photon polymerization (2PP), a process that can be used to sensitize photorefractive polymers.[19] 2PP is an additive fabrication process that occurs through nonlinear interaction of femtosecond laser pulses with photosensitive resin. A femtosecond laser beam is focused with a variable pulse energy. The reaction occurs only in the central region of the focal spot where the laser intensity exceeds the 2PP threshold. As this process is additive, the solidification occurs in a point-by-point basis where the intensity is the highest in the two-photon interaction.

Femtosecond laser machining through direct writing is similar to 2PP in that it applies multi-photon absorption at localized laser intensities that exceed an ionization threshold, but is confined below the material's upper limit ablation threshold. Direct writing is not confined to two-photon absorption but can have three or four photon absorption to induce ionization. The multi-photon absorption is confined to a region near the focal point where the laser intensity exceeds a critical value above which multi-photon absorption allows for modification of the local physical and chemical properties. Multi-photon absorption produces charge as the material is illuminated, ultimately leading to refractive index modulation in a localized area through the increase of the material density in a write location and the color-center formation.[20–22] Beam interference with

femtosecond lasers has also been used to holographically fabricate gratings.[23] The ability to localize material alterations allows experimenters to control the depth of the gratings, allowing for multi-layer gratings. Laser-driven microexplosions can contribute to the formation of a diverse array of periodic nanostructures.[24]

Recently, experimentation with femtosecond laser machining has been directed towards transparent materials for applications including waveguide fabrication, functional devices, diffractive optical elements, and photonic crystals.[25] This is particularly promising, as the high intensity confines material alterations to the focal volume as a result of nonlinear absorption processes. Changes are caused by laser-induced optical breakdown as the energy is transferred to the electrons in the material, which then transfer energy to the lattice, resulting in a microplasma. Such interactions produce a localized change in the refractive index of the sample.[3] The process is extremely precise due to minimized heat diffusion outside of the focal area. Thus, femtosecond machining has far-reaching implications for nanofabrication of three-dimensional devices.

Using a femtosecond laser to produce such structures offers many advantages. The process requires fewer steps and less equipment than traditional methods that require cleanroom usage. Devices can be rapidly prototyped since the process relies on software control as opposed to masks necessary for photolithography which are time and cost intensive, and femtosecond machining lends itself to three-dimensional processing, providing a significant advantage over traditional methods.[26] In the development of our femtosecond machining device we first must characterize the required material limits.

3. PRINCIPLES AND PHYSICAL CHARACTERISTICS OF DIRECT WRITING WITH A FEMTOSECOND LASER

High-precision material micromachining is achievable when the dominant mechanism is a physical control of the energy rather than a thermally dominated process. If the heat energy is distributed across a large area, then the heat affected zone washes out the efficiency of the micromachining tool's spot size. The electron-phonon coupling strength defines the thermalization of a material in the conversion time to transfer energy from the electron to the material lattice in terms of heat and energy. Materials exhibit an electron-phonon coupling strength of $1 - 100$ ps (1×10^{-12} s to 1×10^{-10} s), which is longer than the operation time of a femtosecond pulse of $1 - 100$ fs (1×10^{-15} s to 1×10^{-13} s).[16] This shorter pulse duration allows for electron energy to dominate the micromachining process as it takes a few hundred femtoseconds to a few picoseconds for materials to reach thermal equilibrium when irradiated with a femtosecond pulse.[27] Microfabrication becomes realizable as a majority of the laser energy operates in a non-thermal process. The thermal diffusion length, or length of heat effects when a material reaches its melting point by femtosecond laser irradiation, is given by

$$l_d = \left(\frac{128}{\pi} \right)^{1/8} \left(\frac{DC_i}{\gamma^2 T_{im} C'_e} \right)^{1/4} \tag{1}$$

Where D is the thermal conductivity, C_i is the lattice heat capacity, C'_e is given by $C'_e = C_t/T_e$ (where C_e is the electron heat capacity and T_e is the electron temperature), and γ is the electron-phonon coupling constant.[28] The heat emission is often times in the length of nanometers, which is within the wavelength of the emitted laser light.

As electron excitation or ionization is the dominant process over thermalization in the microfabrication machining process, it is important to characterize the energy conversion. It is already established that short energy pulses are outputted in order to overcome the thermalization of a material. These laser outputted short energy pulses are high intensity to overcome the laser's internal activation threshold. To put this into perspective, the relative intensity of a single pulse of power at a 100 fs pulse duration at 1 mJ of power outputs 1×10^9 W or 1 GW of power, whereas a 10 ns pulse duration outputs 100 kW or 1×10^5 W of power. In this calculation, the power is the pulse energy J divided by the pulse duration τ_{pulse}. This increase for the light-matter interaction of high intensity optical energy induces nonlinear optical effects. The characterization of the optical process for femtosecond microfabrication machining is identified through three nonlinear optical mechanisms: 1) multi-photon ionization or multi-photon absorption, 2) tunneling ionization, and 3) avalanche breakdown.

Multi-photon absorption or multi-photon ionization is the primary nonlinear process for electron excitation of a localized spot. Traditional absorption occurs through single photon absorption at a lower energy state. There are additional states such as that of the second energy state and higher absorption states. The actual energy achieved through transition can be calculated through the nonlinear optical susceptibility where the atomic wavefunction obeys the time-dependent
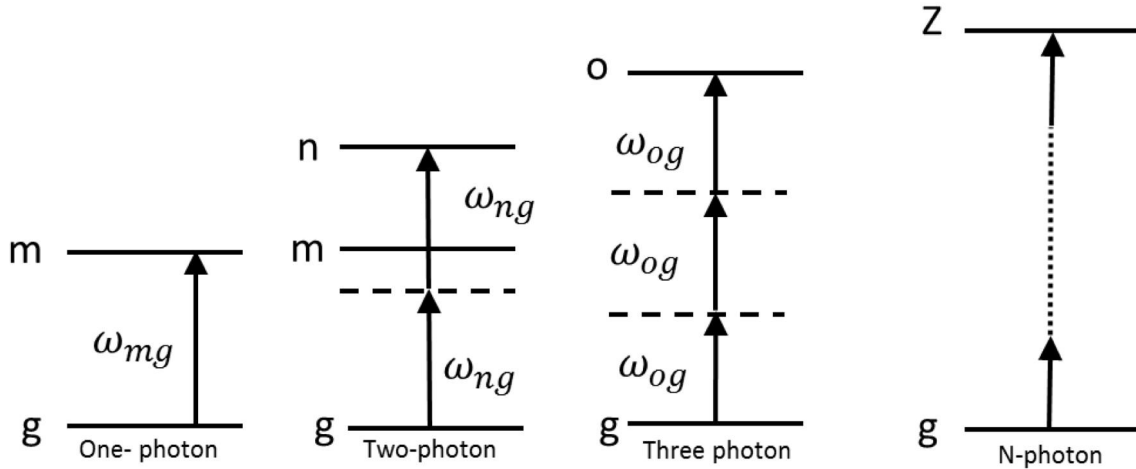
Figure 2. The transition of a single photon absorption state as is observed relative to multi-photon absorption states. A physical view of the change in frequency required to transition to higher energy states.

Schrodinger equation. Each phase transition can be referenced in terms of its absorption cross section where first order transitions linearly with time and the two-photon cross section in terms of a square intensity function and so on. This process enables one to apply the following absorption transition rates of energy absorption at the four lowest absorption terms $R_{mg}^{(1)}(\omega)$ (linear), $R_{ng}^{(2)}(\omega)$ (two-photon), $R_{og}^{(3)}(\omega)$ (three-photon), and $R_{pg}^{(4)}(\omega)$ (four-photon) of the multi-photon absorption function:

$$R_{mg}^{(1)}(\omega) = \frac{p_m^{(1)}}{t} = \frac{|\mu_{mg}E|^2 t}{\hbar^2} 2\pi\rho_f\left(\omega_{mg} - \omega\right) \qquad (2)$$

$$R_{ng}^{(2)}(\omega) = |\sum_m \frac{\mu_{nm}\mu_{mg}E^2}{\hbar^2(\omega_{mg} - \omega)}|^2 2\pi\rho_f\left(\omega_{ng} - 2\omega\right) \qquad (3)$$

$$R_{og}^{(3)}(\omega) = |\sum_m \frac{\mu_{on}\mu_{nm}\mu_{mg}E^3}{\hbar^3(\omega_{ng} - \omega)(\omega_{mg} - \omega)}|^2 2\pi\rho_f\left(\omega_{og} - 3\omega\right) \qquad (4)$$

$$R_{pg}^{(4)}(\omega) = |\sum_m \frac{\mu_{po}\mu_{on}\mu_{nm}\mu_{mg}E^4}{\hbar^4(\omega_{og} - \omega)(\omega_{ng} - \omega)(\omega_{mg} - \omega)}|^2 2\pi\rho_f\left(\omega_{og} - 4\omega\right) \qquad (5)$$

The term $\rho_f(\omega_{mg} = \omega)$ suggests the density of final states is to be evaluated at the frequency ω of the incident laser light. Each frequency is evaluated for a given electric field E where intensity is given by $I = 2n\epsilon_0 cR|E|^2/\omega\hbar$ where ω is the laser frequency, I is the laser intensity, m_e is the electron effective mass, $\hbar$ is Planck's constant, c is the speed of light, n is the linear refractive index, and ϵ_0 is the permittivity of free space. For the absorption terms the tensors μ_{nm}, μ_{mg}, μ_{nm}, and μ_{mg} are of the order of $ea_0 = 8\text{x}10^{-30}$ Cm and $\Gamma_n = 2\pi * (10^{13})$ rad/sec. We also assume that the laser frequency is tuned to the peak of the two-photon resonance, so that $\rho_f(\omega_{ng} = 2\omega) \approx (2\pi\Gamma_n)^{-1}$, where Γ_n is the width of level n. In these evaluations one can observe that the functional variable term in the absorption of photons is the electric field, where tuning the electric field enables the control of the multi-photon absorption. The electric field is tuned through a variation in the input intensity. Multi-photon absorption is achieved across these multiple energy transitions. High density of photons incident on a material can induce an electron transition when excited by multiple photons, even when the band gap exceeds the photon energy.

A further advantage of femtosecond micromachining is in the narrowing of the spatial beam profile of higher order absorption beams. The femtosecond laser already offers higher spatial resolution than alternatives through a suppression of heat energy transition. The linear spatial profile for direct single photon absorption is a Gaussian profile. This base profile narrows as the absorbed energy distribution falls off relative to multi-photon absorption. The fall-off in spot size is
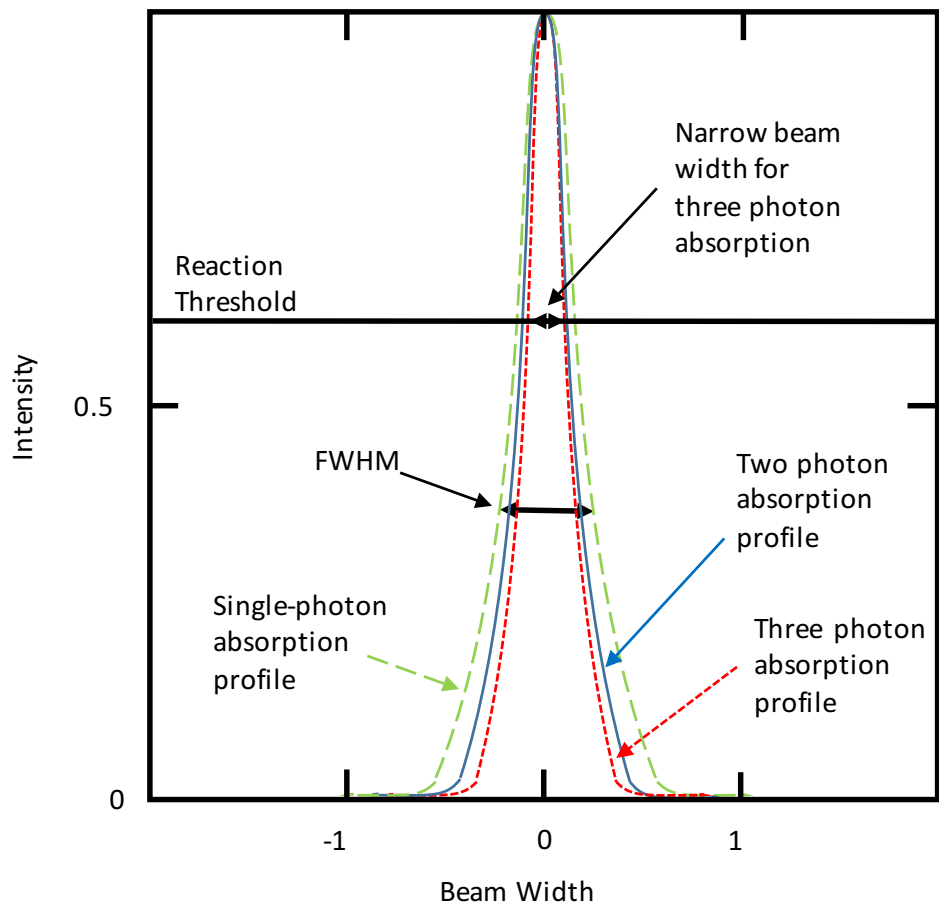
Figure 3. Actual beam profile of the absorption profiles. The spatial distributions of absorbed laser energy narrows from a Gaussian towards a Lorentzian at higher photon absorption values. For a given reaction threshold the smallest spot size is observed from the highest photon absorption profile.

proportional to the nth power of the laser intensity. The effective beam size β for the nth-photon absorption is expressed as $\beta = \beta_0/\sqrt{n}$, where β_0 is the spot size of the focused laser beam at an n absorption level. The combination of the reduced heat and higher absorption levels enables micromachining to optimize spatial resolution of an absorbed point.

The two constructive nonlinear processes that cause material photo-ionization for femtosecond micromachining are multi-photon absorption and tunneling ionization. Tunneling ionization occurs at high laser intensities and low frequencies. The higher intensities cause the electric field to break down the quantum well's symmetry. The fields that are normal to the bulk material observe the Franz-Keldysh effect or the DC Stark effect with possible red-shifting. The potential barrier is no longer symmetric, which causes an elimination in the following of the strict transition and selection rules. The voltage overcomes the coulomb potential that when coupled with the lower of symmetry enables ionization for electrons to reach the conduction band from the valence band. This tunneling through the lowered wall of the quantum well is known as tunneling ionization. This effect becomes more common as the intensity of the field is increased.

The probabilities of multi-photon absorption and tunneling ionization in femtosecond laser interaction with transparent materials can be determined by the Keldysh parameter, γ:[29]

$$\gamma = \frac{\omega}{e}\sqrt{\frac{m_e c n \epsilon_0 E_g}{I}} \qquad (6)$$

Where ω is the laser frequency, I is the laser intensity, m_e is the electron effective mass, e is the fundamental electron charge, c is the speed of light, n is the linear refractive index, ϵ_0 is the permittivity of free space, and E_g is the band gap of the material. Multi-photon absorption is the dominant non-linear process for photo-ionization when γ is much greater than 1. Inversely, when g is much smaller than 1 tunneling ionization is the dominant nonlinear process for photo-ionization. When $\gamma \approx 1$ photo-ionization is induced by a combination of both processes.[17]

Photo-ionization for femtosecond laser micromachining occurs when either the nonlinear process of tunneling ionization or multi-photon absorption is applied, but when does the material break down? Optically induced damage ultimately limits the maximum amount of power that can be transmitted through a particular optical material. As an upper threshold, optical damage limits the maximum field strength E that can be used to excite the nonlinear response. This in turn constrains the nonlinear process to an intensity where material ablation or vaporization occurs. In femtosecond laser micromachining this is an important threshold. Above the optical damage threshold the micromachining device cuts and vaporizes the material. Below this threshold one can alter the refractive index without destroying the material. There is a further lower limit in energy where the photon energy is smaller than the band gap triggering no absorption in the stationary state and thus no ionization occurs.

There are three nonlinear processes that induce optical damage to reach the optical damage threshold limit, where the dominating nonlinear process is variant on the approximate energy.[16] Avalanche breakdown is the dominant mechanism of material breakdown for pulse lasers shorter than the 1 μs pulse range, which is the range the femtosecond laser falls within. The laser intensity that avalanche breakdown operates in is in the 10^9 W/cm^2 to 10^{12} W/cm^2, which is also in the intensity range in which many femtosecond lasers operate. The next nonlinear regime that dominates in the material breakdown is multi-photon ionization where at this intensity range of 10^{12} W/cm^2 to 10^{16} W/cm^2 optical materials over ionize and vaporize. The third dominant breakdown regime is for intensities greater that 10^{16} W/cm^2 caused by what is known as direct field ionization. In direct field ionization the laser field strength rips electrons away from the atomic nucleus as the laser field strength is stronger than the atomic field strength. This third nonlinear regime has not been observed for laser pulses longer than 100 fs.

The avalanche breakdown is a nonlinear phenomenon that is the dominant damage mechanism for most pulsed lasers. A small number of free electrons within the optical material are accelerated to high energies through their interaction with the laser field. The few electrons within the material are created by thermal excitation, tunneling ionization, multi-photon ionization, or free electrons from material defects on the surface. A cascading or avalanche effect occurs where the free electrons ionize other atoms within the material. This in turn further outputs additional electrons that are accelerated to quicken ionization until a complete material breakdown occurs. On the surface of the bulk thermal excitation, tunneling ionization, multi-photon ionization and surface defects accelerate the avalanche breakdown causing surface ablation. As we enter further into the bulk material there is a reduction in the avalanche breakdown with the same matching intensity as there are fewer terms in the avalanche breakdown with a focus on tunneling excitation and multi-photon excitation. Therefore at the same laser intensity one would ablate at the surface or would densify the material bonding in the bulk to alter the
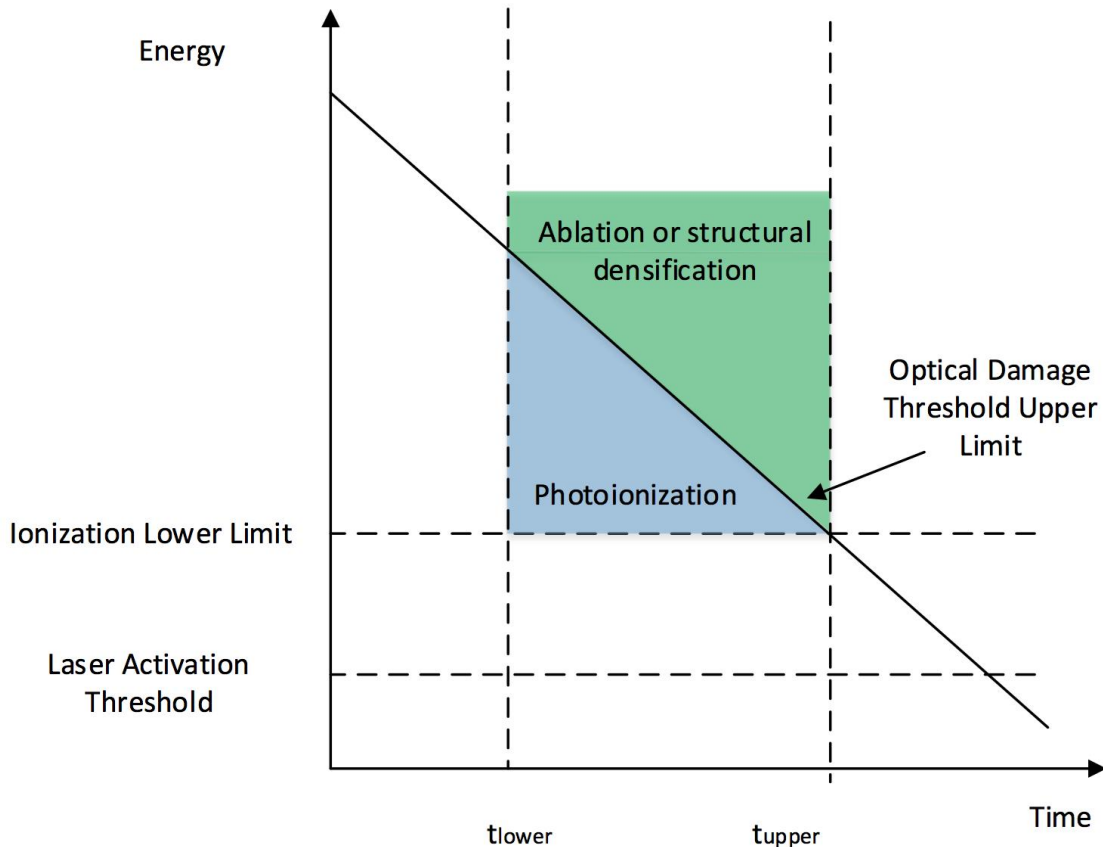
Figure 4. A basic functional understanding of the energy separation between photoionization, which is a combination of multi-photon absorption and tunneling ionization, relative to a threshold that induces material breakdown of either structural densification or ablation.

refractive index. For example, a depth of 15 μm is required to write directly on a silicon wafer.[6] The exact mechanism for the depth requirement has not been fully determined by the scientific community,[30,31] but from an understanding of the avalanche breakdown it is highly probable that the reduction in cascading causes the variation in these two phenomena.

4. MICROMACHINING TOOL FOR REFRACTIVE INDEX MODIFICATION OF LITHIUM NIOBATE

We have explored the mechanisms that allow femtosecond micromachining to function and now we explore the application of the micromachining tool towards refractive index modification for producing waveguides. The energy transferred through bond breaking and densification increases the refractive index of most materials. There are a few materials where the bond breaking decreases the refractive index but that is not in the scope of our current lithium niobate material. It is established that due to the fundamental process of femtosecond lasing refractive index variation, it is only possible to alter the refractive index within a bulk material rather than on the surface. Refractive index variation within materials enables waveguides to be achieved where there is a control in the refractive index between the core center and the cladding sides.[3] Studies have been performed to determine the optimal femtosecond micromachining setup for developing waveguides within bulk materials.[6] There are two separate types of setups that are optimal depending on the intended type of refractive index. A high repetition rate in the order of the MHz range coupled with a low peak power laser pulse enables an isotropic refractive index change in the bulk. If, however, one would like to produce an anisotropic refractive index change so as to create birefringent refractive index material in the bulk, then one would create a femtosecond laser micromachining setup with a KHz repetition rate and high peak power.

Currently the target is to produce and optimize a continuous isotropic refractive index change in lithium niobate. This target is achievable with a MHz high repetition rate and low peak power laser pulse. We have built a Ti:Sapphire based
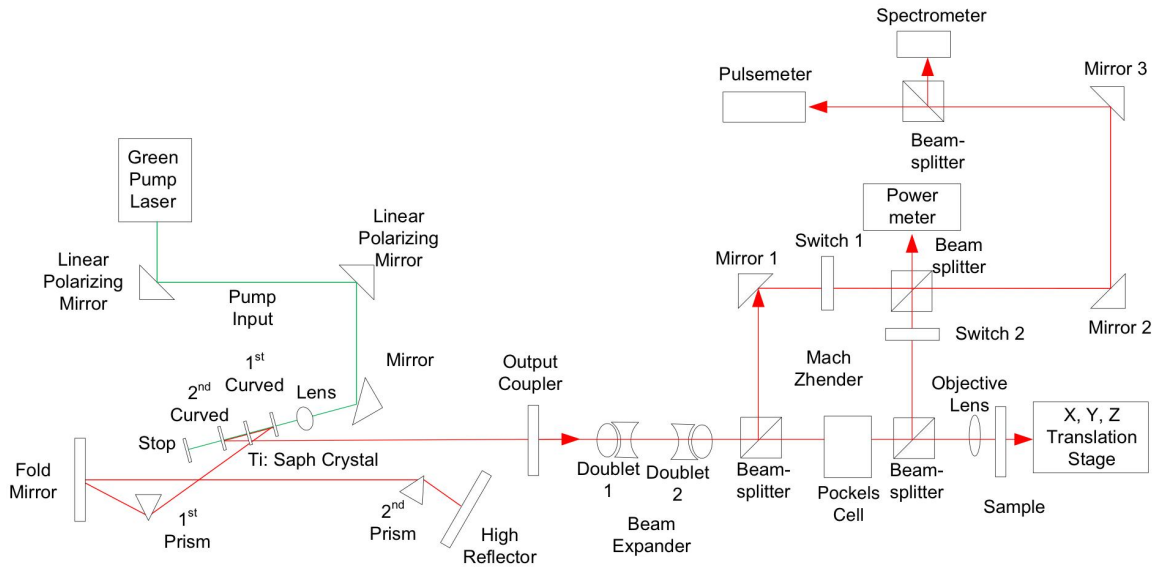
Figure 5. Current optical setup of the femtosecond micromachining setup where we simultaneously control and measure laser intensity, time duration, and wavelength tunability. We also permit multiple degrees of freedom to alter Numerical Aperture (NA) and other optical configurations for improved micromachining.

femtosecond laser that operates at 85 MHz. The laser has a low peak power of approximately 400 μW and is tunable. This base femtosecond laser system is tunable through an additional Pockels cell system that allows for the reduction of power to 0 μW offering the micromachining control of tuning the light intensity from 0 μW to 400 μW.

There are five primary parameters that affect the resolution and thus the accuracy of our point ionization. These parameters are: 1) The spot size due to the NA of the objective lens, 2) the light intensity, 3) the exposure time, 4) the wavelength of the femtosecond pulses, and 5) material selection. We developed a system that controls all five of these primary parameters. As was, stated the light intensity is controllable through the Pockels cell. The system's NA is controlled through the objective lens. Currently we applied a high NA achromatic lens as our objective lens with a 20 mm focal length and a 20 mm diameter offering an NA of 1. It is preferred to apply high NA lenses with the lower power as they offer a shorter depth of field and enable one to focus on a smaller spot.

The exposure time can be controlled indirectly through two mechanisms built into the system to control this term. One mechanism in controlling the exposure time is the traditional way of physically shifting the x,y,z translation stage. The speed determines the amount of time a material is exposed. The second mechanism is controlling the intensity of the beam through the Pockels cell. Here we apply a constant rate as we shift positions on the x,y,z translation stage. The maximum intensity matches the peak intensity of the femto laser energy where vaporization or ablation occurs within the material. The Pockels cell controls the intensity from a range below ablation to a point below ionization. Within this intensity range the material's refractive index is altered in the structural densification intensity region. Additionally, we allow tunability to below the initial ionization levels. This dynamic range enables us to determine various amounts of photoionization and determine the effects that these low intensities have on our resolution spot. This double mechanism approach enables both mechanical and charge-based mechanisms to control the exposure time.

The final parameters that are controllable are the wavelength and bandwidth of the wavelength pulse. We have the ability to tune the high reflector and the out coupler to tune our wavelength and the pulse width. There are built in mechanisms to determine the changes in our wavelength band and our pulse width. A spectrometer is added to determine the spectral range of our femtosecond lasers output band. The output power of the femtosecond laser is simultaneously measured to identify the change in intensity. Concurrently, a frequency-resolved optical gating (FROG) device is added to determine the variation pulse width while we perform writing and system alterations.

As a first order verification that our femtosecond micromachining tool is functioning properly we micro-machined a silicon slide. The current slide shows locations where ablation occurred in cutting across the surface of the slide. Ablation offers a visual indicator that the femtosecond micromachining setup is able to write on a material. The next step will
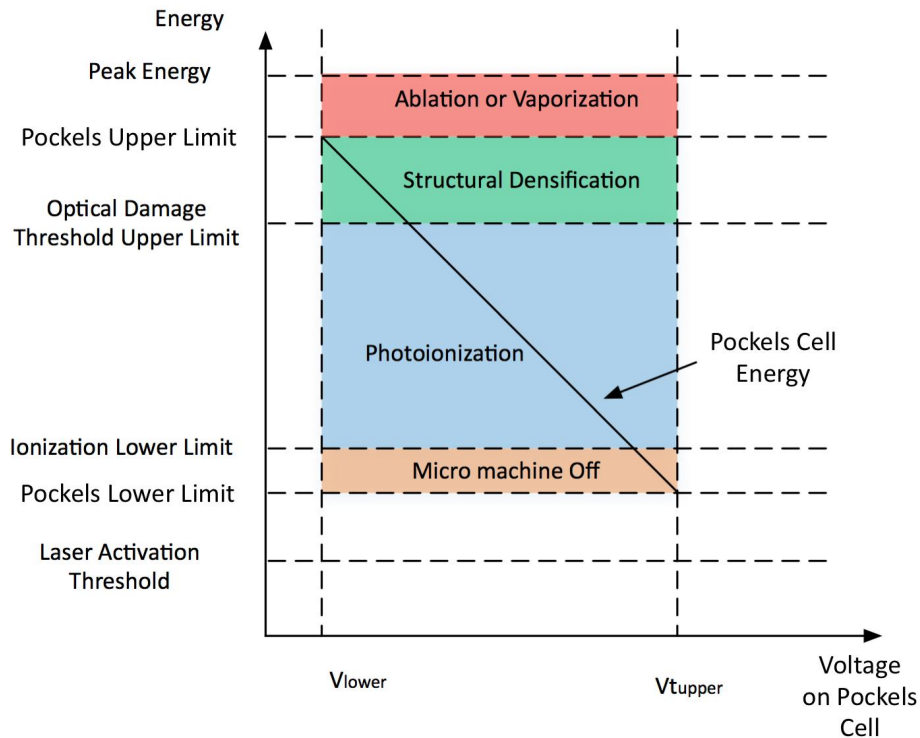
Figure 6. Exposure time is controlled for in each location by tuning the intensity with the Pockels cell rather than scanning across the surface. The Pockels cell tunes the intensity through a voltage input between an artificial off position which below the ionization energy of a material to a position where structural densification can occur to induce a change in refractive index.

be to establish the proper metrology tools to measure the refractive index variation while fabricating the sample. The addition of metrology tools imbedded into the micromachining tool would enable real time measurements of the sample. Metrology tools would enable us to characterize the refractive index changes in addition to identify power variations on the sample. A further step would be to add a Mach-Zehnder interferometer to be able to backtrack a variation in the refractive index. Additionally, post-processing metrology measurements would allow for a verification in the change in material properties. Raman spectroscopy would allow for a determination of the structure. Diffractometry methods would enable us to determine localized wavefront variations. Additionally, a localized interferometric approach such as a Shack-Hartmann wavefront sensor would bring a dimension of identifying local variations instead of an averaged out global measurement that a refractometer or traditional interferometer would achieve.

5. CONCLUSIONS

In this paper, we explored femtosecond laser micromachining as an alternative to proton exchange in the fabrication of waveguides for anisotropic leaky-mode modulators. The direct writing of the femtosecond micromachining will streamline the process. The results achieved to date illustrate the first steps towards achieving femtosecond micromachining of our anisotropic leaky-mode modulators.
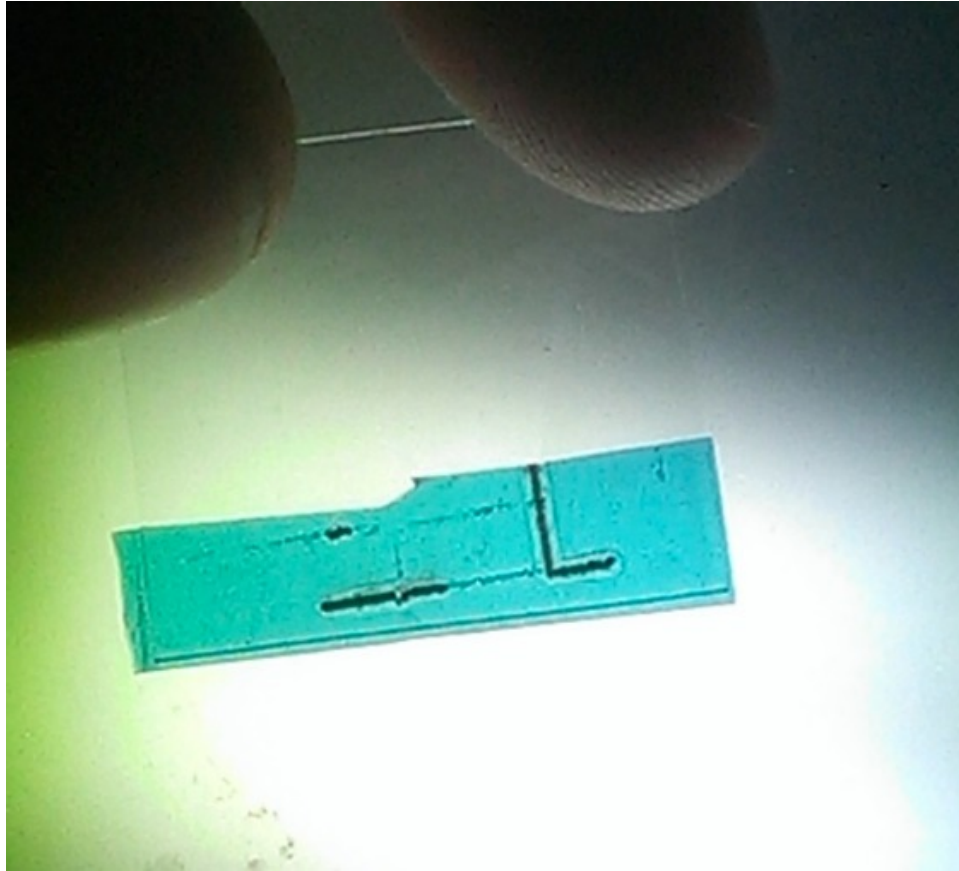
ACKNOWLEDGMENTS

Figure 7. Here the femtosecond laser exhibits the capability to reach high enough intensities to ablate glass. An additional tape was ablated to show contrast. With the system capable of ablating it is functionally capable of achieving the slightly lower energy requirement of structural densification.

REFERENCES

[1] D. Smalley, Q. Smithwick, V. M. Bove, Jr., J. Barabas, S. Jolly, "Anisotropic leaky-mode modulator for holographic video displays," *Nature*, vol. 498, pp. 313-317, 2013.

[2] D. Smalley, Q. Smithwick, J. Barabas, V. M. Bove, Jr., S. Jolly, and C. Della Silva, "Holovideo for everyone: a low-cost holovideo monitor," *Proceedings of the 9th International Symposium on Display Holography*, 2012.

[3] K. M. Davis, K. Mira, N. Sugimoto, and K. Kirao, "Writing waveguides in glass with a femtosecond laser," *Optics Letters*, vol. 21, p. 1729, 1996.

[4] E. N. Glezer, M. Milosavljevic, L. Huang, R. J. Finlay, T. H. Her, J. P. Callan, E. Mazur, "Three-dimensional optical storage inside transparent materials," *Optics Letters*, vol. 21, 2023, 1996.

[5] P. P. Pronko, S. K. Dutta, J. Squieir, J. V. Rudd, D. Du, and G. Mourour, "Machining of sub-micron holes using a femtosecond laser at 800 nm," *Optics Communications*, vol. 114, no. 106, 1995.

[6] P. Yang, G. Burns, J. Palmer, M. Harris, K. McDaniel, J. Guo, G. A. Vawter, D. R. Tallant, M. L. Griffith, and T. S. Luk., "Microfabrication with Femtosecond Laser Processing: (A) Laser Ablation of Ferrous Alloys, (B) Direct- Write Embeded Optical Waveguides and Integrated Optics in Bulk Glass," *Sandia Report*, Sandia National Labs, November 2004.

[7] K. Sugioka and Y. Cheng, "Femtosecond laser processing for optofluidic fabrication," *Lab on a Chip*, 12:3576-3589, 2012.

[8] F. Chen, "Photonic guiding structures in lithium niobate crystals produced by energetic ion beams," *Journal of Applied Physics*, vol. 106, 081101, 2009.

[9] R. He, Q. An, Y. Jia, G. R. Castillo-Vega, J. R. V. De Aldana, and F. Chen, "Femtosecond laser micromachining of lithium niobate depressed cladding waveguides," *Optical Materials Express*, vol. 3, 1378-84, 2013.

[10] S. Kroesen, W. Horn, J. Imbrock, and C. Denz, "Electro-optical tunable waveguide embedded multiscan Bragg gratings in lithium niobate by direct femtosecond laser writing," *Optics Express*, vol. 22, 23339-48, 2014.

[11] J. Burghoff, H. Hartung, S. Nlte, and A. Tunnermann, "Structural properties of femtosecond laser induced modifications in LiNbO3" *Applied Physics A*, 86, 165-70, 2006.

[12] V. Guarepi, C. Perrone, M. Aveni, F. Videla, G. A. Torchia, "Bending waveguides made in x-cut lithium niobate crystals for technological applications," *Journal of Micromechanics and Microengineering*, vol. 24, no. 12, Nov. 2015.

[13] M. R. Tejerina, D. A. Biasetti, and G. A. Torchia, "Polarization behavior of femtosecond laser written waveguides in lithium niobate," *Optical Materials*, vol. 47 , pp. 34-38, 2015.

[14] J. LV, Y. Cheng, W. Yuan, F. and Chen, "Three dimensional femtosecond laser fabrication of waveguide beamsplitters in LiNbO3 crystal," *Optical Material Express*, vol. 5, 1274-1280, 2015.

[15] R. R. Thomson, S. Campbell, I. J. Blewett, A. K. Kar, and D. T. Reid, "Optical waveguide fabrication in z-cut lithium niobate (LiNbO3) using femtosecond pulses in the low repetition rate regime," *Applied Physics Letters*, 88, 111109, 2006.

[16] R. W. Boyd, *Nonlinear Optics*. 3rd edition, Academic Press, 2008.

[17] K. Sugiokax and Y. Cheng, "Femtosecond laser 3D Micromachining for Microfluidic and Optofluidic Applications," *Springer Briefs in Applied Sciences and Technology*, Springer, 2014.

[18] R. Gattass, and Eric Mazur, "Femtosecond laser micromachining in transparent materials," *Nature Photonics*, v. 2, pp. 219-225, 2008.

[19] S. Tay, et al, "Photorefractive polymer composite operating at the optical communication wavelength of 1550 nm," *Applied Physics Letters*, v 85, pp.4561-4563, 2004.

[20] P. A. Blanche, et al, "Photorefractive polymers sensitized by two-photon absorption," *Optics Letters*, v. 27, pp 19-21, 2002.

[21] W. J. Reichman, D. M. Krol, L. Shah, F. Yishino, A. Arai, S. Eaton, P. Herma, "A spectroscopic comparison of femtosecond-laser-modified fused silica using kilohertz and megahertz laser systems," *Journal of Applied Physics*, 99, 123112, 2006.

[22] C. Ponader, J. Schroeder, and A. Streltsov, "Origin of the refractive index increase in laser written waveguides in glasses," *Journal of Applied Physics* 103:063516(5), 2008.

[23] Y. Li, et al, "Holographic fabrication of multiple layers of grating inside soda-lime glass with femtosecond laser pulses," *Applied Physics Letters*, v. 80, pp. 1508-1510, 2002.

[24] K. Kawamura, et al, "Periodic nanostructure array in crossed holographic gratings on silica glass by two interfered infrared-femtosecond laser pulses," *Applied Physics Letters*, v. 79, 2001.

[25] S. Hasegawa and Y. Hayasaki, "Holographic femtosecond laser processing with multiplexed phase fresnel lenses displayed on a liquid crystal spatial light modulator," *Optical Review*, v. 14, pp. 208-213, 2007.

[26] G. Della Valle,, R. Osellame, and P. Laporta, "Micromachining of photonic devices by femtosecond laser pulses," *Journal of Optics A: Pure and Applied Optics*, v. 11, 2009.

[27] C. K. Son, F. Vallee, L. H. Acioli, E. P. Ippen, J. G. Fujimoto, "Femtosecond-tunable measurement of electron thermalization in gold," *Physical Review B*, 50, 15337, Nov. 1994.

[28] P. B. Corkum, F. Brunel, N. K. Sherman, T. Srinivasan-Rao, "Thermal Response of Metals to Ultrashort-Pulse Laser Excitation," *Physical Review Letters*, vol. 61, 2886, 1988.

[29] L. V. Keldysh, "Ionization in field of a strong electromagnetic wave," *Soviet Physics JETP*, 20:1307-1314, 1965.

[30] G. Y. Yang and Y. R. Shen, "Spectral broadening of ultrashort pulses in a nonlinear medium," *Optics Letters*, 9(11) 510-512. 1984.

[31] A. Broder, S. L. Chin, "Band-gap dependence of the ultrafast white-light continuum," *Physical Review Letters*, 80(20) 4406-4409. 1998.

[32] R. Osellame et al, "Femtosecond laser writing of waveguides in periodically poled lithium niobate preserving the nonlinear coefficient," *Applied Physics Letters*, v. 90, pp. 241107-241107, 2007.

[33] M. N. Armenise, "Fabrication techniques of lithium niobate waveguides," *IEE Proceedings Journal on Optoelectronics*, v. 135, pp. 85-91, 1988.